Joint PhD Project∓
Mechanical analysis in the morphogenesis of fish embryos

PhD Student: Paulo C. Godolphim[1,2]

Supervisor Professors: Rodrigo Soto[2], Leonardo G. Brunnet[1]

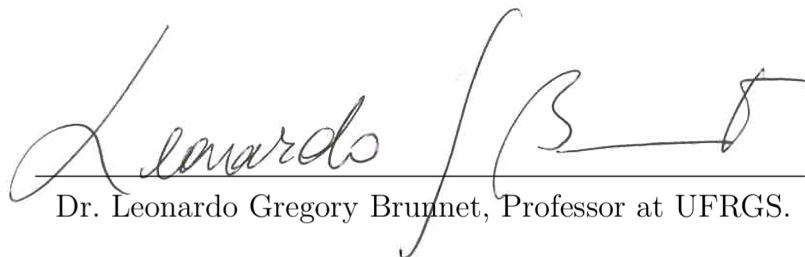[1] *Instituto de Física, Universidade Federal do Rio Grande do Sul, Porto Alegre, Brazil.*

[2] *Departamento de Física, FCFM, Universidad de Chile, Santiago, Chile.*

(January 27, 2022)

∓ This plan is part of a joint PhD agreement between the physics departments of *Universidad de Chile* (UChile) and *Universidade Federal do Rio Grande do Sul* (UFRGS). The parties involved sign this document below:

_____

Me. Paulo Casagrande Godolphim, PhD Student.

_____

Dr. Rodrigo Soto, Professor at UChile.

_____

Dr. Leonardo Gregory Brunnet, Professor at UFRGS.

Abstract

Understanding how a small number of cells grows into a fully differentiated animal, i.e., morphogenesis, is an interdisciplinary problem with applications from robotics to disease treatment. Determining tissue dynamics' physical and mechanical nature is essential to construct a complete picture of how animals develop. The objective of this project is to combine continuum mechanics theory, particle simulations, and *in vivo* experimental data to understand how endogenous mechanical forces and tissue patterns correlate to morphological events in the epiboly process of *Annual Killifish* and *Zebrafish* embryos morphogenesis. To ensure the relevance of our results, the models chosen to extract

1

mechanical properties of the tissue will be quantitatively validated for each individual cell in a calibrating process called *micro-mechanics*. This work is mostly based and inspired by the PhD thesis of Fernanda Pérez-Verdugo [1]. Moreover, the work will be done in collaboration with the LEO laboratory, led by Prof. Miguel Concha, at Faculty of Medicine of the *Universidad de Chile*, responsible for the experimental data.

1   Introduction

The impact of material science in the modern world is undeniable. Understanding the underlying physical equations behind materials like steel, concrete and semiconductors enabled us to build our cities and technology. Now a new field is emerging where we try to understand biological tissue, i.e., collectives of cells working together to perform some task, as *biological materials*. These materials have fundamental mechanical equations that yet need to be found, tested, and defined. The future applications of this science will span from developing life-like materials to robotics, organs printing, understanding diseases development and progression (like birth diseases and cancer), and the development of new treatments. There are several ongoing works trying to reach does goals, but there is still much work to be done.

The study of biological materials poses an extra difficulty in relation to its more classical counterpart. The combination of physics and material engineering with biology and medicine introduces an inherent complexity to this subject. Consequently, the physicist's efforts are generally focused on experiments with reduced complexity like *in vitro* cellular monolayers [2, 3, 4, 5, 6, 7, 8, 9], *in vitro* cellular aggregates [10, 11, 12, 13], and *in vivo* morphogenesis experiments of model animals [14, 15, 16, 17, 18, 19, 20]. The last ones are of particular relevance in medicine and biology, since *in vivo* assays, although more complex than *in vitro* ones, generally give results with more real-life applications. However, this extra complexity makes it harder to obtain a complete picture of these systems, especially regarding the mechanical aspects of the tissue.

The knowledge of how biochemical signals drive an organism's growth has advanced significantly with the genomics revolution. Nevertheless, the mechanical side is still lacking in understanding. Moreover, although it is known that both biochemical and mechanical signals play a crucial role in animal development, how these different mechanisms work together is not fully understood. A practical case of the previous is in the epiboly process during morphogenesis of the *Annual Killifish* and the *Zebrafish* embryos [21, 22]. Although these two fishes are widely used as model animals to understand animal development, there is still much to be known of how the force transmission drives the evolution of these systems.
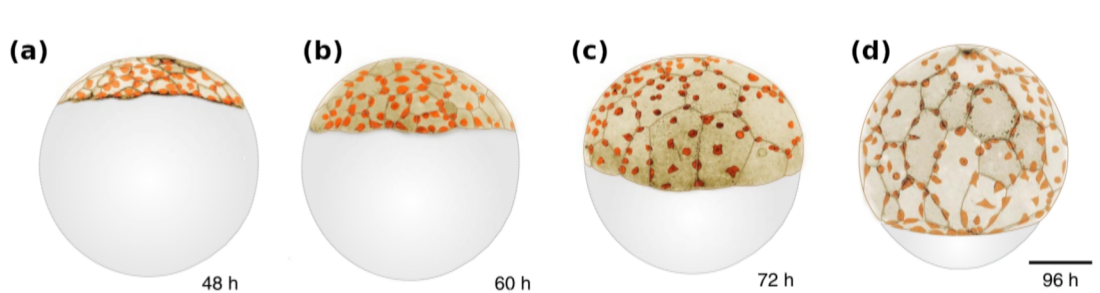

Figure 1: Epiboly process in the *Annual Killifish* (adapted from Ref. [21]).

2

The epiboly is one of the initial embryonic stages of the *Annual Killifish*, and the *Zebrafish*, where the embryo is in a spherical shape with an internal part called *yolk* and an external layer of cells (EVL) that spread over the yolk. In Figure 1 (a), we can see the pre-epiboly[1] where the EVL cells (in brown) are packed together in the pole over the yolk (in gray). The EVL will then spread until all the yolk is covered (Figure 1 b, c, and d). This is accomplished by the cells actively decreasing their height, and doing so, increasing their surface area. Moreover, after they cross the equator, two other active processes come to play: the contraction of a supracellular ring of proteins formed in the border of the EVL and a traction of microtubule cables that stretch from the south pole of the yolk to the edge of the EVL. How this different mechanism directs the epiboly is unclear. Moreover, the EVL in the *Killifish* shows contraction pulses, and in the *Zebrafish* there are also contraction events that lead to delaminations, i.e., when a cell detach from the EVL and enter the internal part of the embryo. These two processes are important morphological events in which the relation with the forces in the system is not clear. All these open questions are well suited for an analysis from the mechanical point of view.

Cells are discrete and independent active objects. However, the description of tissues as a continuum-like material has proven successful in obtaining mechanical properties. In Ref. [8], by modeling an epithelial monolayer as an active nematic liquid crystal, they show that high-stress regions in the tissue are precursors of cell extrusion and cell death. In Ref. [20], by using supracellular actin fibers in the *Hydra* as nematic director of a continuous field, they show that the appearance of morphological structure, e.g., the mouth and tentacles of the animal, are associated with topological defects. In Refs. [19] and [18], using a continuum mechanics approach, where the cells in the tissue are treated as polygons (with vertices and edges) of a continuum material, they were able to correlate strain and stress patterns, obtained from the modeling, with morphological events in the wing and the thorax of the *Drosophila*, respectively.

From experiments to theory, there is no shortage of tools to analyze the mechanical aspects of tissues. Refs. [23], and [24] present a robust theoretical framework to describe discrete patterns, like foams bubbles and cells, as a continuum material, and then, retrieve mechanical observables. Refs. [25] and [26] present a comprehensively reviews of experimental techniques used to quantify forces in biological tissues, being *traction force microscopy* [27, 28] the most used one, probably. Nevertheless, when considering real three-dimensional *in vivo* scenarios, measuring forces is yet a troublesome and expensive process, and, sometimes, because of the specificity of each biological problem, requires also the development of a new technology. To overcome this experimental problem, numerical models are widely used as solutions. One simulates the tissue and tries to extract from the model's predefined dynamics and constitutive laws of the model, the mechanical properties in the tissue.

There are several numerical models in biology. One of the most used for tissues is the *Vertex Model* [29, 30, 31, 32, 33, 34, 35, 36, 37], which is a relatively simple, but powerful particle model. A recent and more complex approach is the *deformable particle model* (or *ring model*) [38, 39, 40], that have been used to describe soft solids and single cells, but a tissue application is still lacking. To ensure that the dynamical observables extracted from the models have a real relevance to the target experiment, they must be calibrated and validated by the experimental data. Although approaches in this direction are already being made, a thorough and quantitative validation of these models in *in vivo*

---

[1]Figure 1 shows only the epiboly process for the *Annual Killifish*, however, the process is very similar for the *Zebrafish*.

situations is still necessary.

In this work, we want to determine if stress and strain patterns are mechanical precursors for morphological events, namely, cellular contractile pulses and delimitation, in the *Annual Killifish* and *Zebrafish* epiboly process. Also, we want to investigate how the different active forces, namely, cellular height decrease, supracellular contraction ring, and microtubule related traction, work together to drive cells during epiboly. We aim to achieve these goals by analyzing the data from three-dimensional *in vivo* experimental images as a continuum mechanics problem and by comparing the experiments with the vertex model and the deformable particle model. We also aim to introduce micromechanics, a validation process where the model's accuracy in predicting the tissue's motion is tested for each individual cell, as a quantitative validation technique for tissue models. Using the validation, we aim to determine if the general form of the vertex and deformable particle models are indeed a good representation of biological tissue. If they are not a good representation, we will show how we must modify these models to fit the experiments correctly.

The strain patterns will be computed directly from the experimental tissue displacement field by using small deformation elastic theory [41]. In contrast, the forces in the system, necessary ingredients to compute the stress, will be obtained indirectly from the validated numerical models. The stress tensor of the cells will be derived from kinetic theory [42]. Finally, after having the validated models and the mechanical fields, we will attempt a complete simulation of the whole epiboly process to understand the different active forces in the system.

This work is relevant because our mechanical analysis will help complete the big picture of how animals evolve. Also, the validation process may have a high impact in the tissue physics field since several works use the vertex model. Moreover, micro-mechanics is a general technique that could validate current and future models in tissue biology.

2 Objectives

GO[2]: Compare the dynamics of the enveloping epithelial cell layer in the morphogenesis of fish embryos to two discrete models for biological tissues: the vertex model and the deformable particle model.
SO1: Quantitatively validate the well-established vertex model using experimental data to find the most appropriate form for the models' equations and the values of the parameters.
SO1.1: Repeat the validation in **SO1** for the less known deformable particle model and compare the results with those of the vertex model.
SO2: Use the validated models and elastic theory to map the stress and strain patterns in the experiments to determine if there is a correlation between mechanical inhomogeneities or anisotropies in the tissue and morphogenic events, like delamination and cell contractile pulses. That is, investigate if stress and strain inhomogeneities or anisotropies are precursors or proxies of morphological events in fish embryos.
SO3: Use the validated model to investigate the role and the interplay of the different active forces that drive the epiboly process in fish embryos.

---

[2]**GO** - General Objectives; **SO** - Specific Objectives

3 Experimental data and Models

3.1 Experimental data

Our data consists of 3D *in vivo* experiments, developed by the LEO laboratory, led by Prof. Miguel Concha, at Faculty of Medicine of the *Universidad de Chile* of the *Annual Killifish* and the *Zebrafish* epiboly process. The displacement of the cells in the samples is a slow process, with characteristic times on the scale of hours. The fast frame rate and the good resolution of the images enable capturing the tissue in detail.

In the movie 01, we can see the pre-epiboly process in the *Annual Killifish*. The more external cells are increasing in area while spreading over the Yolk. In the movie 02, we can see the zebrafish cells migrating, while conserving the area, in the last part of the epiboly process. From the experiments, we can extract observables, such as, the borders of the cells, the area of the cells, the perimeter, and the vertices, i.e., the points where the cellular membranes of three (or more) cells connect, as can be seen in Fig. 2. We will use these observables to compute the tissue displacement field and calibrate the numerical models. In movie 03, we see the 2D digital reconstruction of the experimental data from the vertices of the Killifish embryo (only the edges connecting the vertices are shown). In movie 04, we see the 2D projection of the experimental raw data from the borders of the cells from the same experiment.

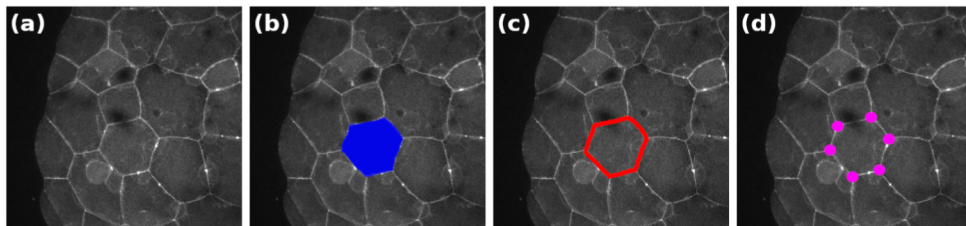Figure 2: (a) Snapshot of the *Annual Killifish* cells. (b,c,d) The observables: area, perimeter and vertices of the same cell.

3.2 Vertex model

In the vertex model, as the name indicates, we simulate the dynamics of vertices of cells rather than the cells themselves. The simulated tissue then is not composed of individual point-like cells but as a collection of vertices where the off-lattice $\mathbf{r}_i$ position of each vertex evolves in time according to an energy functional E of the entire tissue. Since a biological tissue is an over-damped system, the motion of the vertices will be given by Eq. (1):

$$\gamma \frac{d\mathbf{r}_i}{dt} = -\frac{\partial E}{\partial \mathbf{r}_i},$$ (1)

where γ is the drag constant of the system. The basic structure of the tissue is given by its associated graph G:

$$G = \{\text{Vertices, Edges, Cells}\}_{\text{IDs}},$$ (2)

a set of vertices, edges, and cells IDs that determine the topology of the tissue. Figure 3 (a) shows a generic graph of a tissue. The graph structure in the vertex model is arbitrary and can have a constant topology or not, depending on the objective of the simulation. In our case, the graph, and hence, the topology, is defined by the experimental data.

Although the topology is not necessarily fixed for the entire time of the experiments (for example, cell division or delamination events), in our initial approach we will only work with sections of the tissue that conserve topology over time.
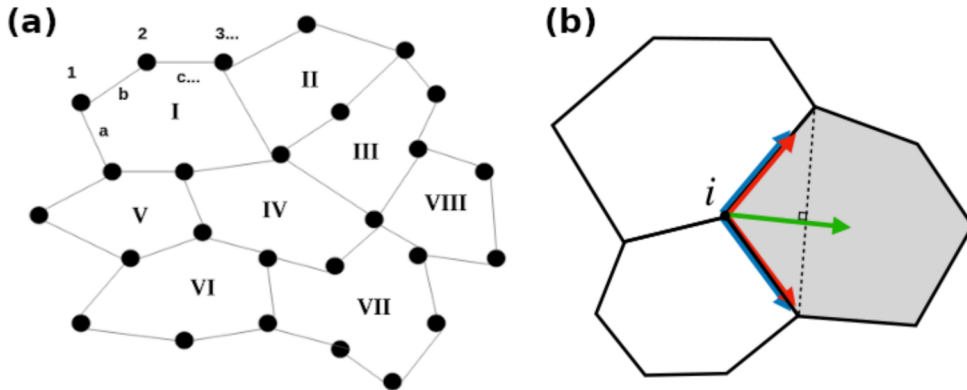

Figure 3: **(a)** A generic vertex tissue graph comprising eight cells (roman numbers). In this graph, the edges a, b and c and the vertices 1 and 2 belong to the cell I, and the vertex 3 belong to both cell I and II. **(b)** Representation of the force vectors over the vertex i associated with the gray cell. Green is the area force vector, and red and blue are the perimeter, and line tension force vectors (adapted from Ref. [1]).

Just like the Graph structure, the energy functional in Eq. (1) can have an arbitrary shape. Many modelings try to account for the 3D design of the cells constructing a 3D graph for the tissue where, in general, the energy functional will try to conserve properties like the volume and surface of the cells [34]. However, more straightforward 2D approaches [29] show both qualitative and quantitative agreement with experiments in whats is called *apical models*: a model where the tissue is simplified as only the top part, or the top view of the cells. When considering biological tissues with constant topology, especially epithelial tissues, like the ones studied here, the following form is commonly used:

$$E = \sum_c \frac{K_A}{2} \left(A_c - A_{0c} \right)^2 + \sum_c \frac{K_P}{2} (P_c - P_{0c})^2 + \sum_{\langle i,j \rangle} J_{i,j} l_{i,j}, \tag{3}$$

where Eq. (3) describes a 2D planar tissue, and K_A, K_P, and $J_{i,j}$ are parameters of the model.

Equation (3), applied to Eq. (1), dictates that the vertices will move to minimize the tissue energy so that the area A_c and the perimeter P_c of each cell are the closest as possible to the target area A_{0c} and perimeter P_{0c}. The third term in Equation (3) introduces a *line tension* to the system, associated with each of the $l_{i,j}$ edges connecting each i, j pair of vertices, resulting in an attractive-only (for $J_{i,j} > 0$) or repulsive-only (for $J_{i,j} < 0$) force between the vertices that generally acts against the other two equilibrium terms.

Each term in Eq. (3) has a biological interpretation. Assuming that the 3D volume of the cells is constant in time, the area term, with elastic modules K_A, represents the resistance to height fluctuations, i.e., the incompressibility of the cell. The incompressibility is due to the conservation of the fluid inside the cell (mostly water) and to the overall actomyosin structure of the cell cytoskeleton. With elastic module K_P, the perimeter term is associated with the actomyosin ring that forms in the apical part of the cell. In [29], using $P_{0c}=0$, the perimeter term is given the interpretation of an always enduring

contraction force of this ring of proteins. In Ref. [1], by letting A_{0c} and P_{0c} change in time, the area and the perimeter term give the interpretation of active myosin-driving contractility forces with medial and perimetral origin, respectively. Finally, the line tension term, with force module $J_{i,j}$, represent the adhesion cost energy. Assuming that the density of adhesion is constant along the cells' borders, a bigger $l_{i,j}$ means more adhesion, and so, more adhesion energy in that segment, which is modeled using $J_{i,j} > 0$.

Inspecting Eq.(3) we see that the perimeter and the line tension term have similar mathematical origins. Considering a periodic system with $J_{i,j} = J$, i.e., the limit of an infinity large tissue with uniform line tension, and knowing that $P_c = \sum_c l_c$, we can rewrite the energy functional as:

$$E = \sum_c \frac{K_A}{2} (A_c - A_{0c})^2 + \sum_c \frac{K_P}{2} \left[P_c - \left(P_{0c} - \frac{J}{2K_P} \right) \right]^2 - \sum_c \left(\frac{J^2 - 4JP_{0c}K_P}{8K_P} \right). \quad (4)$$

The last term in Eq. (4) has only constants and so it vanishes when applied to Eq. (1), while $\left(P_{0c} - \frac{J}{2K_P} \right)$ is equivalent to a new target perimeter P_{0c}^* that depends on the ratio between J and K_P. Consequently, although the perimeter and the line tension terms have distinct biological and physical meanings, when regarding the mathematical motion of the vertex, the line tension can be absorbed to the perimeter term, resulting in the simplified functional form:

$$E = \sum_c \frac{K_A}{2} (A_c - A_{0c})^2 + \sum_c \frac{K_P}{2} (P_c - P_{0c})^2, \quad (5)$$

where we changed the name of the variable P_{0c}^* back to P_{0c} for simplicity. The experimental data contains only some dozens of cells, being far from an infinity tissue. However, we will use Eq. (5) as our initial attempt to model the tissue-based in the Occam's razor logic. If necessary, we will consider more complex functionals, such as Eq. (3). Nevertheless, we expect that Eqs. (3) and (5) will only show significantly different results for the case that the line tension in the tissue is not uniform. For example, in the epiboly final stage, where a contractile supracellular ring of proteins is formed in the opposite pole of the yolk. The contraction forces of the ring could then be easily modeled using Eq. (3), e.g., by increasing the values of $J_{i,j}$ of the edges belonging to the supracellular ring.

Finally, to account for increasing apical size of the cells, i.e., the area of the cells, in time, resulting from the cell's spread to cover the yolk (see movie 01), we will add a plastic dynamic for the target area and perimeter:

$$\frac{dA_{0c}}{dt} = -\nu_A (A_{0c} - A_c) + f_A, \quad (6)$$

$$\frac{dP_{0c}}{dt} = -\nu_P (P_{0c} - P_c) + f_P, \quad (7)$$

where ν_A and ν_P are the plastic rates in which the target area A_{0c} and perimeter P_{0c} relax to the instantaneous values of area A_c and perimeter P_c, and f_A and f_P are expansion functions for the area and perimeter, which will be given by the experimental data.

3.3 Deformable Particle Model

In the deformable particle model, we define the cell explicitly as a ring of particles connected via a set of potential energies that make the cell conserve specific quantities, such

7

as area and perimeter, but allow it to deform softly [38, 39, 40]. Figure 4 shows a illustration of a cell in this model. In contrast to the vertex model, the tissue assumes a more discrete structure. Each of the individual cells has an independent dynamic, and the cohesiveness of the tissue will depend on the explicit interaction laws chosen between the particles, i.e., between the membranes of the cells.
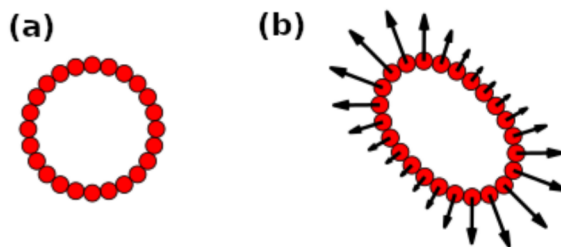

Figure 4: (a) A deformable particle with 24 vertices in a circular shape. (b) Example of a deformation. In black we see the resulting curvature vectors associated to this shape. Adapted from Ref. [38].

Each cell in the model can be interpreted as an polygon with N vertices closed packed together. The energy functional of a tissue of deformable particles will be given by:

$$E = \sum_c \frac{K_A}{2} \left(A_c - A_{0c}\right)^2 + \sum_c \frac{K_L}{2} \sum_i (l_{ic} - l_{0c})^2 + \sum_c \frac{K_B}{2} \sum_{i \in c} (l_{i,i-1})^2 + E_{\text{int}}, \qquad (8)$$

where l_{ic} is the length of the edge connecting the vertices i and $i+1$ of cell c, and $l_{i,i-1}$ is the module of the curvature vector given by the difference between the edge vectors of three subsequent vertices of a same cell: $\mathbf{l}_{i,i-1} = \mathbf{l}_i - \mathbf{l}_{i-1}$. The first term is equivalent to the area term in Eqs. (3) and (5). The second term is similar to the perimeter term in the same equations. The third term is the bending energy, which gives the model extra stability under deformations. The last term E_{int} is the interaction energy between different cells, which is generally modeled as a short-range attraction force.

One of the advantages of the deformable particles is the possibility of the explicit study of cell-cell adhesions, an essential aspect of tissue dynamics. Moreover, in many situations in the experiments, the border of the cells will be curved. The deformable particle model does not face any relevant problem in this case (see movie 5[3]), while the vertex model would need to be modified to account for such a feature. However, these extra features come with the cost of being a computationally slower model than the vertex one, since a tissue of deformable particles may have about ten times more particles than the vertex model.

Although the deformable particle and vertex models are intrinsically different models, in both of them, we can compute the same required observables, e.g., cell area, perimeter, anisotropy. Consequently, the quantitative validation process used will be the same.

4   Methodology: Quantitative Validation

The validation of the models will follow the premise: if the model equation is an accurate description of the biological tissue, then it must be valid for each part of the tissue and for

---

[3]Gustavo Ourique, private communication.

the whole tissue at the same time. The procedure for doing this quantitative validation using cell-by-cell analysis is called Micro-mechanics. Here we will use the vertex model as a reference to explain the procedure, but it is supposed to be an equivalent process for the deformable particle model.

4.1 Quantitative validation via micro-mechanics

In a quantitative validation, one seeks to match the values of observables in the experiment and in the theoretical/numerical model by fitting the model with experimental data. The procedure is then to test a set of different values for the parameters in the model, e.g., K_A, K_P, ν_A, ν_P, to minimize a functional for the entire tissue:

$$F = \int dt \sum_c \left[\left(A_c^{\text{exp}} - A_c^{\text{sim}} \right)^2 + a \left(P_c^{\text{exp}} - P_c^{\text{sim}} \right)^2 \right], \qquad (9)$$

and also to minimize N other functionals for each of the N cells in the tissue:

$$F_c = \int dt \left[\left(A_c^{\text{exp}} - A_c^{\text{sim}} \right)^2 + a \left(P_c^{\text{exp}} - P_c^{\text{sim}} \right)^2 \right], \qquad (10)$$

where a is a constant that sets A and P to have the same units and same contribution for the functionals. If the model is a good description of the experiments, then the set of optimal parameters obtained from Eqs. (9) and (10) should have approximately the same values.

Equation (10) is probably the simplest functional we will use. Nevertheless, due to a greater number of degrees of freedom for a cell, i.e., $2n$ for n vertex, than the number of constraints, i.e., two (the area and the perimeter), it may be necessary to include additional terms in the functional. For example, we could add a constrain in the edges of the cells, like $\sum_i \left(l_i^{\text{exp}} - l_i^{\text{sim}} \right)^2$, to minimize the distances l_i between all the vertex belonging to the target cell. Another alternative could be to minimize also in relation to the j neighbors cells of the target cell i:

$$F_{c_i} = \int dt \left\{ \left(A_{c_i}^{\text{exp}} - A_{c_i}^{\text{sim}} \right)^2 + a \left(P_{c_i}^{\text{exp}} - P_{c_i}^{\text{sim}} \right)^2 + \sum_j \left[\left(A_{c_j}^{\text{exp}} - A_{c_j}^{\text{sim}} \right)^2 + a \left(P_{c_j}^{\text{exp}} - P_{c_j}^{\text{sim}} \right)^2 \right] \right\}, \qquad (11)$$

which will increase the number of constraints and decrease the possibility of degenerated states, e.g., rotated cells with the same shape.

Other functional forms can be thought of for this minimization. Still, it is crucial to consider the cost-to-effect relation, i.e., how much more time demanding is the implementation in relation to the gain in fit accuracy. Moreover, it is essential to check if the newly added terms have redundancy. For example, since the perimeter is computed as the sum of the l_i edges, adding an edge minimization could have some redundancies with the perimeter minimization, leading to a lower number of constraints than expected. Since the minimization process does not depend on the explicit form of the functional, we will consider the simpler Eq. (10) to continue the explication.

4.2 Quantitative validation via micro-mechanics: details

The validation quality depends strongly on the quality of the experimental data and on the number of samples, i.e., the number of embryos times the number of cells in each

embryo. In Figure 5 (b,c,d), we can see three snapshots of the pole of the *Annual Killifish* embryo in the pre-epiboly showing the evolution in time of a cell.

In Figure 5 (a), we can see a digital reconstruction of the initial configuration of the tissue from the experimental data. This reconstruction is a tissue of 39 cells that represent the bulk of the tissue (because of the way the vertex model is written, in the validation we can only work with experimental vertices that are entirely surrounded by cells). Using the data from Figure 5 (a) as the initial condition, one could then can simulate the entire bulk of the tissue with the vertex model using the experimental data of the surface cells (the cells surrounding the bulk, not shown in the figure) as boundary conditions. In this sense, we have an actually simulated passive tissue (the bulk) that is driven by an interpolated (not simulated) active tissue (the surface) given by the experiments. Using this approach, we can run simulations for different sets of parameters until we find the optimal set of parameters for the whole tissue that evolve the simulation as close as possible to the experimental data, i.e., the parameters that best minimize the functional in Eq. (9).
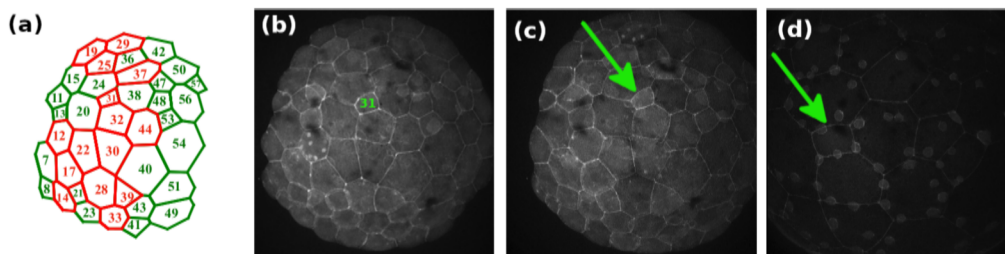

Figure 5: **(a)** Digital reconstruction of the experimental data in **(b)** (adapted from Ref. [1]). **(c,d)** Showing the same cell for early times and later times in the experiment, respectively.

Having the best-fitted simulation, one can derive the forces inside the tissue from the dynamic equations of the model. Movie 6 shows the force field obtained for the experiment shown in Figure 5 (the color map is the intensity of the forces)[4]. Assuming a high quality in the fitting procedure, it is undeniable that the mechanical fields obtained using this approach will be a relevant result. However, an important question remains: how do we know if the stress pattern found is indeed a good representation of the mechanical forces inside the tissue? In other words, it is possible, and even likely, that given enough parameters, one can fit not just one model to an experiment but several. Then, how can we know which one is the correct mechanical description of the experiments?

A solution would be to execute mechanical experiments to validate the model. Still, the central idea of using a numerical model for tissue is to avoid, when possible and wise, doing real and expensive experiments. Here we will try to solve this problem using the micro-mechanics approach.

In the micro-mechanics approach, rather than simulate the entire tissue, we simulate only a small portion of it, e.g., one cell (see Figure 6), and for that one cell, that we can call $C1$, we minimize the functional in Eq. (10) to obtain the optimal set of parameters for cell $C1$, i.e., we obtain: $\text{set}_{C1} = (K_{A,C1}, K_{P,C1}, \nu_{A,C1}, \nu_{P,C1})$. We repeat this for cells $C2$, $C3$, ..., C_N, until we have a general set $\{set_{Ci}\}$ with the optimal parameters for each of the cells in the tissue. The model will be considered an accurate description of the biological tissue if the optimal parameters of all cells have approximately the same value. In movie 7, we can see the micro-mechanics simulation for one cell. The simulated part of
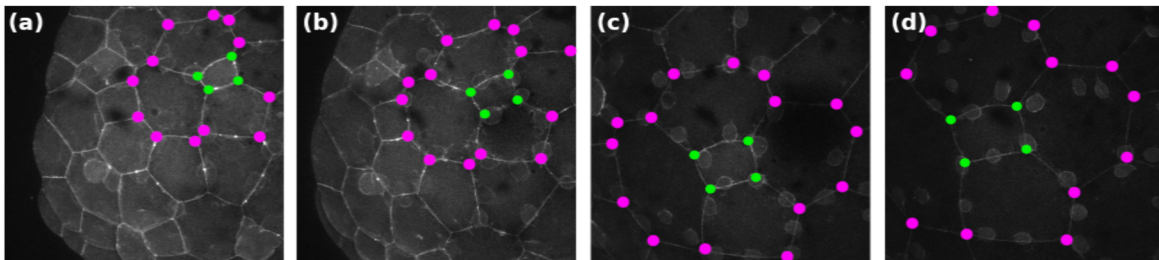
---

[4]Fernanda Perez, private communication.

Figure 6: The green vertices corresponds to the cell that will be simulated via micromechanics. In contrast, the purple ones correspond to the surrounding cells, for which the experiments give the evolution. The time in the experiment is increasing from **(a)** to **(d)**.

An excellent way to understand this validation is to think about the Navier-Stokes equation. We know that the Navier-Stokes is a good model for some fluid because we have quantitative experimental measurements showing that each part of the fluid obeys the state equation. This experimentally based validation is what we want to do to model our biological tissue. Suppose we find that the set of optimal parameters differs from each other. In that case, the next step will be to modify the model to find the "correct" form of the equations, similarly to adjusting the Navier-Stokes to account for a turbulent fluid, for example.

4.3   Possible outcomes

Since we are in the initial stage of the project, it is not wise to be very speculative. Nevertheless, we believe in three different possible outcomes for the validation. (i) The best-case scenario where the obtained optimal parameters are the same for all cells. (ii) The cells do not have the same parameters, but there is some correlation between the obtained parameters and properties of the cell. For example, the area force constant K_A has a linear relation with the initial target area of the cells. In these cases, the results would be telling us that modifying K_A to $k_A A_{0c}$ is a necessary modification of the model. (iii) The worst-case scenario where the parameters are different, and there is no correlation whatsoever. This situation would probably require rethinking the model from scratch.

5   Methodology: Fate of the Tissue

This section explains how we will extract the endogenous mechanical information, using the validated models and elastic theory, and then try to correlate it to morphological events in the embryos.

5.1   Stress field

The stress tensor σ_c of each of the c cells in the tissue will be computed by the relation:

$$\sigma_c = -\frac{\sum_i \mathbf{R}_i^c \otimes \mathbf{f}_i^c}{A_c}, \tag{12}$$

where the sum is over all the i vertices belonging to the cell, A_c is the area of the cell, $\mathbf{R}_i^c$ is the distance vector between the vertex i and the center of the cell, $\mathbf{f}_i^c$ is the force vector experienced by vertex i, and $\otimes$ is the tensorial product. This relation is derived from Kinetic Theory (Ref. [42], pag. 26) and was used by Ref. [1] to compute the average stress in a vertex model tissue.

Equation (12) has a general form and can be used not only for the vertex model, but also for the deformable particle models. The $\mathbf{R}_i^c$ and the A_c are obtained directly from the experimental images, while the forces $\mathbf{f}_i^c$ will be given as outputs from the simulations.

5.2   Strain field

Although the cells in the tissue undergo large deformations during the experiments, the deformations of the cells between two frames of the experimental data are small. Consequently, we can use the strain tensor for small deformations (Ref. [41], pag. 4) to write the strain tensor ε_c for a cell c as:

$$\varepsilon_c = \frac{1}{2}\left[\nabla\mathbf{u}_c + (\nabla\mathbf{u}_c)^T\right],\tag{13}$$

where $\mathbf{u}_c$ is the displacement field inside the cell c between two frames, $\nabla\mathbf{u}_c$, a rank two tensor, is the gradient of $\mathbf{u}_c$ and $()^T$ is the transpose. We do not know the exact form of $\mathbf{u}_c$, but we can assume a simple linear form for the displacement:

$$\mathbf{u}_c = \mathbf{u}_0^c + \Gamma^c\mathbf{R}_c,\tag{14}$$

where $\mathbf{u}_0^c$ is associated with the translation of the cell, $\mathbf{R}_c$ is the distance between any point inside the cell and the center of the cell, and Γ^c is the deformation matrix of the cell. Applying Equation (14) to Equation (13) we obtain that:

$$\varepsilon_c = \frac{1}{2}\left[\Gamma^c + (\Gamma^c)^T\right],\tag{15}$$

and now we only need to obtain Γ to calculate the strain of the cells.

In equation (14), $\mathbf{u}_c$ and $\mathbf{R}_c$ are going to be given by the experimental data. Consequently, we can obtain $\mathbf{u}_0^c$ and Γ^c by fitting the data, i.e., by writing the following quadratic error function:

$$\chi_c^2 = \sum_i\left[\mathbf{u}_i^c - (\mathbf{u}_0^c + \Gamma^c\mathbf{R}_i^c)\right]^2,\tag{16}$$

for each of the c cells in the tissue, where the sum in i is over the vertices of cell c, and then minimizing it in relation to $\mathbf{u}_0^c$ and Γ^c:

$$\frac{\partial\chi^2}{\partial\mathbf{u}_0^c} = \frac{\partial\chi^2}{\partial\Gamma^c} = 0.\tag{17}$$

Solving the set of equations associated with Equation (17) we can then determine $\mathbf{u}_0^c$ and Γ^c, and consequently, calculate the strain.

6   Methodology: Understanding the driving forces in the morphogenesis of fish embryo

Lastly, if all the other steps in the project go well, and if we have time, we will simulate the entire epiboly process to understand the role of the active forces in the system's

dynamics. This is a more speculative part of the project that we still need to elaborate on better. However, we believe that the active area expansion of the cells can be given by the Eqs. (6) and (7). Also, the supracellular contraction ring could be modeled by increasing the values of the line tension terms J_{ij} for all the edges in the border of the tissue. Moreover, the microtubule contraction could be modeled as an external force acting downwards in the border of the tissue. Most probably, all the dynamics in these simulations would also need to be calibrated with the experimental data.

7   A note: the difference between our work and Ref. [1]

This work is a follow-up of ref 1. Still, our approach and objectives are different. (i) Ref 1, like many works in the literature, assumed the vertex model as an accurate description of the experiment and then fitted it to the experimental data. Here we will validate the assumption using micro-mechanics and test if the vertex model is a good description. (ii) Here, we are also working with a second model, the deformable particle model, that will allow us to explore this system's new features and achieve extra robustness for our results. (iii) Ref 1 did not analyze the stress and strain patterns for the cells in the embryo nor their correlation with morphological events, which is one of the main objectives of this work. (iv) Ref 1 analyzed only the pre-epiboly process (less than 30% of the whole epiboly) for only one embryo and one fish. Here we will analyze the entire process for more embryos and two types of fish.

8   Work Schedule

We already have a Python program, originally written by Fernanda Perez [1], for the vertex model simulation of the epiboly for one embryo of the *Killifish*. We also have the optimal set of parameters for the whole tissue (obtained by Ref. [1]), and we are now searching for the optimal parameters in the vertex model for each individual cell in the embryo. We also have a deformable particle program, written in Python and Fortran. This code was made for a single cell on a planar surface, and so, we still need to modify it to the epiboly multi-cell scenario. We are already finishing the derivation of Eq. (17), and since we already have the required experimental data [1], the strain calculations for the first embryo will be ready soon. After the derivation, getting the strain will be a matter of writing a program to solve the resulting equations numerically. Once the vertex model is validated, we will compute the stress in the first embryo and compare it with the strain field and with the occurrence of the active pulses in the EVL. After the vertex model analysis is completed, we will repeat it for the same embryo using the deformable particle model.

Once having the full description of this first embryo, we will then apply the same methodology for the other samples of *Killifish* and for the samples of *Zebrafish*. We already have data from another *Killifish* embryo and a *Zebrafish* embryo. In addition, our collaborators at the LEO lab will be doing more experiments soon to have a good number of samples for each fish. Since our priority is to have a statistically significantly mechanical description of the embryos, we will only attempt the simulations described in section 6 after having all the embryos analyzed accordingly to sections 4 and 5.

Below we can see a brief description of the tasks in the project, and in Table 1 we can see the expected work schedule for each one:

Task 1: Vertex model micro-mechanics validation for the first embryo;
Task 2: Finish the derivation for the strain and obtain the strain for the first embryo;
Task 3: Modify the deformable particle program for multi-cell;
Task 4: Deformable particle model micro-mechanics validation for the first embryo;
Task 5: Obtain the stress, using the validated models, for the first embryo;
Task 6: Analyze the stress and strain fields found for the first embryo: the tissue fate;
Task 7: Repeat the previous steps for the other embryos.
Task 8: Simulation of the entire epiboly process as described in section 6;
Task 9: Write the thesis;
Task 10: Literature review.

	T1	T2	T3	T4	T5	T6	T7	T8	T9	T10	T11	T12
Task 1	■	■										
Task 2	■											
Task 3	■	■										
Task 4		■	■									
Task 5		■	■	■								
Task 6			■	■	■							
Task 7					■	■	■	■				
Task 8									■	■		
Task 9									■	■		
Task 10	■	■	■	■	■	■	■	■	■			

Table 1: The Table shows the three-year work schedule of the project separated into twelve trimesters (T). The beginning of T1 corresponds to January 2022. The last two trimesters (T11 and T12) are considered extension periods that can be used if the work requires some extra months to be finished.

8.1 Possible difficulties and unseen problems

Setbacks in plans are an expected result in research. New waves of the COVID-19 pandemic could force experimentalists to stop producing new experiments, which will undermine the statistical significance of our results. However, we already have data from two killifish embryos and one zebrafish embryo. So, in the worst-case scenario, we already have data to work with. However, experimentalists are already preparing new experiments. By mid-2022, we will likely have data from three embryos of each fish, which is a reasonable number of replicates for *in vivo* biological experiments (the idea is to have more experiments, though). In addition, each embryo has several cells, which increases our statistics.

Suppose the new experimental data does not come. In this case, let's analyze the ones we already have and then shift our focus to simulating the entire epiboly process, as mentioned in section 6. The difference, in this case, will be that the simulation will not have the experimental data to make the results more relevant. However, as we will be using relatively simple models that will already be validated (at this stage of the work), we are pretty confident in extracting from the simulations important information on the interaction of forces during the epiboly.

Another possible setback is that both models fail in the validation and that we cannot find ways to modify the equations so that they become valid. We believe this is an unlikely scenario, as our preliminary results show that the vertex model is a good description. Even so, if the models fail the validation, this is already a significant result. For example, we will show that one of the most used models in tissue physics is not a good description (the vertex model).

References

[1] Fernanda Laura Pérez Verdugo. *Statistical Properties of a Non-Polarized Active Tissue*. PhD thesis, Universidad de Chile, 2021.

[2] Thomas E. Angelini, Edouard Hannezo, Xavier Trepat, Jeffrey J. Fredberg, and David A. Weitz. Cell Migration Driven by Cooperative Substrate Deformation Patterns. *Physical Review Letters*, 104(16):168104, apr 2010.

[3] Thomas E. Angelini, Edouard Hannezo, Xavier Trepatc, Manuel Marquez, Jeffrey J. Fredberg, and David A. Weitz. Glass-like dynamics of collective cell migration. *Proceedings of the National Academy of Sciences*, 108:4714–4719, 3 2011.

[4] Xavier Serra-Picamal, Vito Conte, Romaric Vincent, Ester Anon, Dhananjay T. Tambe, Elsa Bazellieres, James P. Butler, Jeffrey J. Fredberg, and Xavier Trepat. Mechanical waves during tissue expansion. *Nature Physics 2012 8:8*, 8:628–634, 7 2012.

[5] Sri Ram Krishna Vedula, Andrea Ravasio, Chwee Teck Lim, and Benoit Ladoux. Collective cell migration: a mechanistic perspective. *Physiology*, 28(6):370–379, 2013.

[6] Agustí Brugués, Ester Anon, Vito Conte, Jim H. Veldhuis, Mukund Gupta, Julien Colombelli, José J. Muñoz, G. Wayne Brodland, Benoit Ladoux, and Xavier Trepat. Forces driving epithelial wound healing. *Nature Physics 2014 10:9*, 10:683–690, 8 2014.

[7] Simon Garcia, Edouard Hannezo, Jens Elgeti, Jean-François Joanny, Pascal Silberzan, and Nir S Gov. Physics of active jamming during collective cellular motion in a monolayer. *Proceedings of the National Academy of Sciences of the United States of America*, 112(50):15314–9, dec 2015.

[8] Thuan Beng Saw, Amin Doostmohammadi, Vincent Nier, Leyla Kocgozlu, Sumesh Thampi, Yusuke Toyama, Philippe Marcq, Chwee Teck Lim, Julia M. Yeomans, and Benoit Ladoux. Topological defects in epithelia govern cell death and extrusion. *Nature*, 544:212–216, 4 2017.

[9] Sham Tlili, Estelle Gauquelin, Brigitte Li, Olivier Cardoso, Benoît Ladoux, Hélène Delanoë Ayari, and François Graner. Collective cell migration without proliferation: density determines cell velocity and wave velocity. *Royal Society Open Science*, 5, 5 2018.

[10] Julio M. Belmonte, Gilberto L. Thomas, Leonardo G. Brunnet, Rita M. C. de Almeida, and Hugues Chaté. Self-propelled particle model for cell-sorting phenomena. *Phys. Rev. Lett.*, 100:248702, Jun 2008.

[11] M. Lisa Manning, Ramsey A. Foty, Malcolm S. Steinberg, and Eva Maria Schoetz. Coaction of intercellular adhesion and cortical tension specifies tissue surface tension. *Proceedings of the National Academy of Sciences of the United States of America*, 107:12517–12522, 7 2010.

[12] Michel Moussus, Christelle Der Loughian, David Fuard, Marie Courçon, Danielle Gulino-Debrac, Hélène Delanoë-Ayari, and Alice Nicolas. Intracellular stresses in patterned cell assemblies. *Soft Matter*, 10:2414–2423, 3 2014.

[13] Carine P. Beatrici, Rita M.C. De Almeida, and Leonardo G. Brunnet. Mean-cluster approach indicates cell sorting time scales are determined by collective dynamics. *Physical Review E*, 95(3), mar 2017.

[14] Jos Käfer, Takashi Hayashi, Athanasius F.M. Marée, Richard W. Carthew, and François Graner. Cell adhesion and cortex contractility determine cell patterning in the drosophilaretina. *Proceedings of the National Academy of Sciences*, 104:18549–18554, 11 2007.

[15] Matteo Rauzi, Pascale Verant, Thomas Lecuit, and Pierre François Lenne. Nature and anisotropy of cortical forces orienting drosophila tissue morphogenesis. *Nature Cell Biology 2008 10:12*, 10:1401–1410, 11 2008.

[16] M. Krieg, Y. Arboleda-Estudillo, P. H. Puech, J. Käfer, F. Graner, D. J. Müller, and C. P. Heisenberg. Tensile forces govern germ-layer organization in zebrafish. *Nature Cell Biology 2008 10:4*, 10:429–436, 3 2008.

[17] Benoît Aigouy, Reza Farhadifar, Douglas B. Staple, Andreas Sagner, Jens Christian Röper, Frank Jülicher, and Suzanne Eaton. Cell flow reorients the axis of planar polarity in the wing epithelium of drosophila. *Cell*, 142:773–786, 9 2010.

[18] Boris Guirao, Stéphane U. Rigaud, Floris Bosveld, Anaïs Bailles, Jesús López-Gay, Shuji Ishihara, Kaoru Sugimura, François Graner, and Yohanns Bellaïche. Unified quantitative characterization of epithelial tissue development. *eLife*, 4, 12 2015.

[19] Raphaël Etournay, Marko Popović, Matthias Merkel, Amitabha Nandi, Corinna Blasse, Benoît Aigouy, Holger Brandl, Gene Myers, Guillaume Salbreux, Frank Jülicher, and Suzanne Eaton. Interplay of cell dynamics and epithelial tension during morphogenesis of the drosophila pupal wing. *eLife*, 4, 6 2015.

[20] Yonit Maroudas-Sacks, Liora Garion, Lital Shani-Zerbib, Anton Livshits, Erez Braun, and Kinneret Keren. Topological defects in the nematic order of actin fibres as organization centres of hydra morphogenesis. *Nature Physics 2020 17:2*, 17:251–259, 11 2020.

[21] Germán Reig, Mauricio Cerda, Néstor Sepúlveda, Daniela Flores, Victor Castañeda, Masazumi Tada, Steffen Härtel, and Miguel L. Concha. Extra-embryonic tissue spreading directs early embryo morphogenesis in killifish. *Nature Communications 2017 8:1*, 8:1–14, 6 2017.

[22] Martin Behrndt, Guillaume Salbreux, Pedro Campinho, Robert Hauschild, Felix Oswald, Julia Roensch, Stephan W. Grill, and Carl Philipp Heisenberg. Forces driving epithelial spreading in zebrafish gastrulation. *Science (New York, N.Y.)*, 338:257–260, 10 2012.

[23] F. Graner, B. Dollet, C. Raufaste, and P. Marmottant. Discrete rearranging disordered patterns, part i: Robust statistical tools in two or three dimensions. *The European Physical Journal E 2008 25:4*, 25:349–369, 4 2008.

[24] P. Marmottant, C. Raufaste, and F. Graner. Discrete rearranging disordered patterns, part ii: 2d plasticity, elasticity and flow of a foam. *The European Physical Journal E 2008 25:4*, 25:371–384, 4 2008.

[25] Kaoru Sugimura, Pierre François Lenne, and François Graner. Measuring forces and stresses in situ in living tissues. *Development*, 143:186–196, 1 2016.

[26] Pere Roca-Cusachs, Vito Conte, and Xavier Trepat. Quantifying forces in cell biology. *Nature Cell Biology 2017 19:7*, 19:742–751, 6 2017.

[27] H. Delanoë-Ayari, S. Iwaya, Y. T. Maeda, J. Inose, C. Rivière, M. Sano, and J. P. Rieu. Changes in the magnitude and distribution of forces at different dictyostelium developmental stages. *Cell Motility and the Cytoskeleton*, 65:314–331, 4 2008.

[28] Xavier Trepat, Michael R. Wasserman, Thomas E. Angelini, Emil Millet, David A. Weitz, James P. Butler, and Jeffrey J. Fredberg. Physical forces during collective cell migration. *Nature Physics 2009 5:6*, 5:426–430, 5 2009.

[29] Reza Farhadifar, Jens Christian Röper, Benoit Aigouy, Suzanne Eaton, and Frank Jülicher. The influence of cell mechanics, cell-cell interactions, and proliferation on epithelial packing. *Current Biology*, 17:2095–2104, 12 2007.

[30] D. B. Staple, R. Farhadifar, J. C. Röper, B. Aigouy, S. Eaton, and F. Jülicher. Mechanics and remodelling of cell packings in epithelia. *The European Physical Journal E 2010 33:2*, 33:117–127, 11 2010.

[31] Dapeng Bi, Jorge H. Lopez, J. M. Schwarz, and M. Lisa Manning. Energy barriers and cell migration in densely packed tissues. *Soft Matter*, 10:1885–1890, 2 2014.

[32] Dapeng Bi, J. H. Lopez, J. M. Schwarz, and M. Lisa Manning. A density-independent rigidity transition in biological tissues. *Nature Physics 2015 11:12*, 11:1074–1079, 9 2015.

[33] Daniel L. Barton, Silke Henkes, Cornelis J. Weijer, and Rastko Sknepnek. Active vertex model for cell-resolution description of epithelial tissue mechanics. *PLOS Computational Biology*, 13:e1005569, 6 2017.

[34] Silvanus Alt, Poulami Ganguly, and Guillaume Salbreux. Vertex models: from cell mechanics to tissue morphogenesis. *Philosophical Transactions of the Royal Society B: Biological Sciences*, 372, 5 2017.

[35] Fernanda Pérez-Verdugo, Jean Francois Joanny, and Rodrigo Soto. Vertex model instabilities for tissues subject to cellular activity or applied stresses. *Physical Review E*, 102:052604, 11 2020.

[36] Shahaf Armon, Matthew S. Bull, Avraham Moriel, Hillel Aharoni, and Manu Prakash. Modeling epithelial tissues as active-elastic sheets reproduce contraction pulses and predict rip resistance. *Communications Physics 2021 4:1*, 4:1–9, 9 2021.

[37] Fernanda Pérez-Verdugo, Germán Reig, Mauricio Cerda, Miguel L. Concha, and Rodrigo Soto. Modelling of active contraction pulses in epithelial cells using the vertex model. 6 2021.

[38] John D. Treado, Dong Wang, Arman Boromand, Michael P. Murrell, Mark D. Shattuck, and Corey S. O'Hern. Bridging particle deformability and collective response in soft solids. *Physical Review Materials*, 5:055605, 5 2021.

[39] Emanuel F. Teixeira, Heitor C.M. Fernandes, and Leonardo G. Brunnet. A single active ring model with velocity self-alignment. *Soft Matter*, 17:5991–6000, 6 2021.

[40] G. Ourique, E.F. Teixeira, and L.G. Brunnet. Modelling micropipette aspiration with active particles. *Physica A: Statistical Mechanics and its Applications*, 589:126661, 3 2022.

[41] Landau y Lifshitz. *Teoría de La Elasticidad*, volume 7. Reverté S. A., 1969.

[42] Rodrigo Soto. *Kinetic Theory and Transport Phenomena*. CLARENDON PRESS - OXFORD, first edition, 2016.